Thin Solid Films 759 (2022) 139467

Contents lists available at ScienceDirect

Thin Solid Films

journal homepage: www.elsevier.com/locate/tsf

Nanoindentation based method to determine the thermal expansion coefficients of low-k dielectrics

Kris Vanstreels *, Abdellah Salahouelhadj, Mario Gonzalez

IMEC, Kapeldreef 75, B-3001 Leuven, Belgium

A B S T R A C T

This paper demonstrates the use of nanoindentation at elevated temperatures to measure the coefficient of thermal expansion (CTE) of low-k dielectric films. This methodology was calibrated using curvature measurements to elucidate the impact of tip geometry and elastic modulus on the theoretical model to calculate the CTE. Further validation was achieved by applying this methodology on a variety of low-k dielectric films with different elastic modulus, but similar matrix density. The advantage of this methodology over other techniques is the capability to simultaneously measure the elastic modulus, the easy sample preparation, short measurement time and easy analysis.

1. Introduction

For many years, the semiconductor industry has continuously improved the functionality and the performance of microelectronic devices of advanced integrated circuits by maximizing the transistor density and continuously scaling the on-chip interconnect wires that link the individual transistors [1–3]. This encouraged the introduction of new materials, processes, packaging strategies, and chip designs into their final products [4,5]. In this context, the implementation of insulating materials with a dielectric constant (k-value) less than that of SiO_2 has become essential for future technology nodes [6]. A common way of decreasing the k-value is by increasing the film porosity. However, this comes at the cost of reduced mechanical properties [7–14]. Furthermore, these dielectric materials must be compatible with the different lithography, stripping, etching and cleaning processes that are used in state-of-the-art integration schemes, together with a sufficient mechanical strength to withstand the high shear stresses and harsh chemical environments that are involved during the chemical mechanical polishing process. On top of that, the coefficient of linear thermal expansion (CTE) is a key parameter in determining how the stress and/or strain develops in interconnect structures during a thermal cycle. The CTE is defined as the fractional increase in length per unit rise in temperature and has been largely ignored for technology nodes of older generations of dielectrics due to their superior mechanical strength over the insulating materials used in advanced nodes. In general, the amount of stress induced in films upon temperature excursions is a function of both CTE and the elastic modulus, so higher CTE for lower modulus films may not be a problem. However, since the CTE of low-k dielectrics can vary widely compared to the surrounding materials used in the integrated circuits and low-k dielectrics exhibit intrinsic tensile stresses, thin film cracking and adhesion are serious thermal-mechanical reliability issues for low-k dielectrics. Therefore, the development of localized and robust CTE methodologies that can be easily applied to new classes of low-k dielectrics films are indispensable. Due to its coupled nature with the elastic modulus and the mechanical link with the substrate where the dielectric is deposited, the CTE of thin films is very difficult to measure without knowing the elastic modulus. The CTE, by definition, must be studied at different elevated temperatures, therefore also knowledge of the elastic modulus at various temperatures is mandatory to accurately extract the CTE. A commonly used approach is to assume that the elastic modulus is not significantly changing over the entire temperature range. However, this may for instance not be the case for polymer materials, which tend to soften at elevated temperatures. On top of that, measuring at elevated temperatures puts stringent demands on the experimental design and its implementation. In literature, there are several available techniques to measure the CTE of bulk materials [15]. In contrast, techniques used to determine the CTE of thin films have rarely been discussed so far [16]. To date, several techniques for measuring the CTE of thin films deposited on a substrate have been developed, which can be mainly divided into four categories: interferometric optical, non-interferometric optical, diffraction-based, and non-optical. Recently, Vanstreels and co-authors have developed a non-optical method to extract the CTE of low-k dielectric films by performing cube corner indentation tests at elevated temperatures and by investigating the fracture behavior of these films at different temperatures [17]. It was found that the cracks that are initiated upon indentation depend on the stress that is generated at the crack tip of crack nuclei, which in turn is composed of the stress induced by the

* Corresponding author.

https://doi.org/10.1016/j.tsf.2022.139467
Received 12 January 2022; Received in revised form 26 August 2022; Accepted 1 September 2022
Available online 5 September 2022
0040-6090/© 2022 Elsevier B.V. All rights reserved.

probe-sample interaction and the film stress before indentation. Since the films stress at a particular temperature T consists of two components, i.e., intrinsic film stress and thermal stress, it was found that the critical force for crack initiation (F_{crit}) changes linearly with temperature,

$$F_{crit}(T) = F_{crit}(T_R) + A_0(T - T_R) \quad (1)$$

Where T_R is the reference temperature, typically room temperature, and the thermal expansion coefficient of a thin low-k film ($\alpha_{Low\text{-}k}$) could then be calculated by

$$a_{lOW-K}(T) = a_{Si}(T) - \left(\frac{1 - \nu_{Low-k}}{E\circ_{Low-k}}\right) \times \left(\frac{A_0}{A_1}\right) \quad (2)$$

where α_{Si} is the CTE of the silicon substrate, $E_{Low\text{-}k}$ and $\nu_{Low\text{-}k}$ are respectively the elastic modulus and Poisson's ratio of the low-k film, and A_1 is defined by

$$F_{crit}(T) = A_1\sigma(T) + A_2 \quad (3)$$

Where σ(T) is the film stress at temperature T and A_2 is the critical force for crack initation at the zero-stress temperature. In the original proposed model, A_1 was determined using finite element modeling (FEM) for a thin film with a fixed elastic modulus and Poisson's ratio and a fixed probe geometry [17]. It was furthermore assumed that the value of A_1 was independent of the probe geometry and the elastic modulus of the thin film material under investigation. In this work, we will demonstrate that A_1 is influenced by the probe geometry and the film's elastic modulus and that an experimental calibration method is required to determine and correct for the dependency of A_1 on the probe geometry and/or the thin film's elastic modulus.

2. Experimental details

A variety of low-k dielectric films were prepared using two different preparation methods. Organosilicate glass (OSG) films with a k-value of 3.0 and 3.2 were deposited by plasma enhanced chemical vapor deposition (PECVD) on 300 mm diameter (100) Si wafers. The deposition temperature was kept at 390 °C. An adjustment of the precursor/gas flow parameters was applied to the deposited OSG films to improve their electrical and mechanical properties including a post-O_2 plasma treatment of 5 s. The film porosity of the OSG 3.0 and OSG 3.2 films was respectively 7% and 5%. The final target thickness of the OSG 3.0 and OSG 3.2 films was approximately 300 nm. For OSG films with a k-value lower than 3.0, an alternative manufacturing sequence was used, as proposed by Urbanowicz et al. [20]. The fabrication process of these OSG films starts with the co-deposition of the organosilica matrix with organic porogen using PECVD on 300 mm (100) Si wafers at 300 °C. Next, the films were treated with a 350 s H_2 after-glow at a wafer temperature of 280 °C using a He/H_2 20:1 downstream microwave plasma treatment in a 300 mm asher from LAM research. Finally, an ultraviolet (UV)-curing step was performed in nitrogen ambient at 430 °C using a narrow-band 172 nm UV-source.

A nanoindentation instrument (TI950 Triboindenter, Bruker) was equipped with two sharp three-sided pyramidal indenter probes to indent and induce radial cracks in the low-k dielectric films under investigation.

The indenter probes have an extended shaft made of a ceramic composite material to maximize the thermal resistance of the probe shaft so that heat conduction through the shaft is negligible. The force and displacement of the nanoindentation probes are simultaneously measured using a three-plate capacitive transducer design, which results in low drift conditions due to heating during electrostatic actuation and hence results in a faster data acquisition with higher accuracy and repeatability can be achieved. Ambient acoustic noise, air currents, laboratory temperature variations, and vibration are minimized through an active and passive damping system and a custom instrument enclosure. Temperature-controlled cube corner indentations were conducted under displacement control mode with predefined maximum penetration depths ranging from 5 nm to 500 nm in an inert gas atmosphere (mixture of 5% hydrogen and 95% nitrogen) using a xSol- 600 temperature stage, which is mounted inside a TI950 triboindenter. When the probe tip enters the heated test chamber prior to performing a measurement, thermal equilibrium between the sample surface and the probe develops within seconds. The xSol-600 temperature stage incorporates a dual, independently controlled heating element architecture that heats from the top and bottom of the sample, forming a micro-environment in the stage's interior, thereby eliminating temperature gradients within the specimen. The thermally stable xSol stage design provides fast stabilization times and a superior feedback-controlled temperature accuracy during the nanoindentation tests of about 0.5 °C.

Curvature measurements are performed optically during thermal treatment, in which a light beam is projected on the sample and the reflected light is collected and analysed to obtain information about the curvature of the sample. From the curvature measurements, estimates of the film stress, thermal mismatch stress, and the CTE of the film are made. Perfect bonding, elastic deformation of the film, and uniform curvature of the coupon are assumed when estimating stress and CTE values from the curvature measurements. The curvature measurement setup contains two main part: an optical head, performing curvature measurements and a vacuum chamber with a sample holder and a heater. The experiments are performed in vacuum, to avoid oxidation and/or interaction of the film with the environment. In addition, the vacuum chamber provides a mechanical support for the sample, optical head and heater. The sample is heated using radiation heat transfer. The heat flux is generated by a halogen lamp, which contains a gold-coated reflector that focuses the light (heat) beam into a spot. The lamp was installed in such a way that the sample is in focal point of the mirror and the focal point is in the center of the sample. The sample holder provides a mechanically stable support for the sample as well as a thermocouple that measures the temperature of the sample during experiments. The curvature measurement principle is based on the two-lens system. Two lenses create an image of an object, where the size of the image is related to the size of the object and the optical magnification of the system (two lenses). The optical magnification is a ratio of the focal length of the two lenses. In the setup, one of the two lenses is replaced with the sample of predefined size (25 mm x 24 mm) which acts as a mirror plane. The size image depends on the size of the object and the ratio of the focal length of the mirror and the known lens. By measuring the size of the object in the focus of the fixed lens, the focal length and curvature of the sample can be obtained. To reduce the curvature measurement noise, a higher number of spots can be used. To allow curvature measurement along X and Y axes, a 2D matrix of spots can be used.

The number of spots (9×9) and size of the single spot (0.5 mm) has been experimentally chosen for optimal noise and data processing time. The experimental setup contains two light sources (Fig. 1). The reference light (REF on Fig. 1) is used to reduce the impact of the imperfections or changes of the GRID. The imperfect distance between holes in GRID and/or changing distance between holes in GRID during experiments (due to e.g. thermal expansion) would introduce an additional error to the curvature measurement result. Therefore, the two light sources are switched during an experiment and two images are captured to obtain the position of the spots. The light that is representing the incident light beam is called REF (e.g. REF LED). The measurement (MEAS) light source generates light that is actually projected and reflected from the sample and it is influenced by the curvature of the sample. During the heating experiment, the light sources are continuously switched on and off. First the REF light source is switched on. The light is collimated and directed to beam splitter, where it is further reflected towards the camera and is not influenced by the sample. It is patterned by the GRID and is captured by the image sensor of the camera. The image is further processed to determine the positions of spots. In this way, the reference positions of the spots are obtained. Subsequently, the REF light source is switched off and the MEAS light source is switched on. The light is

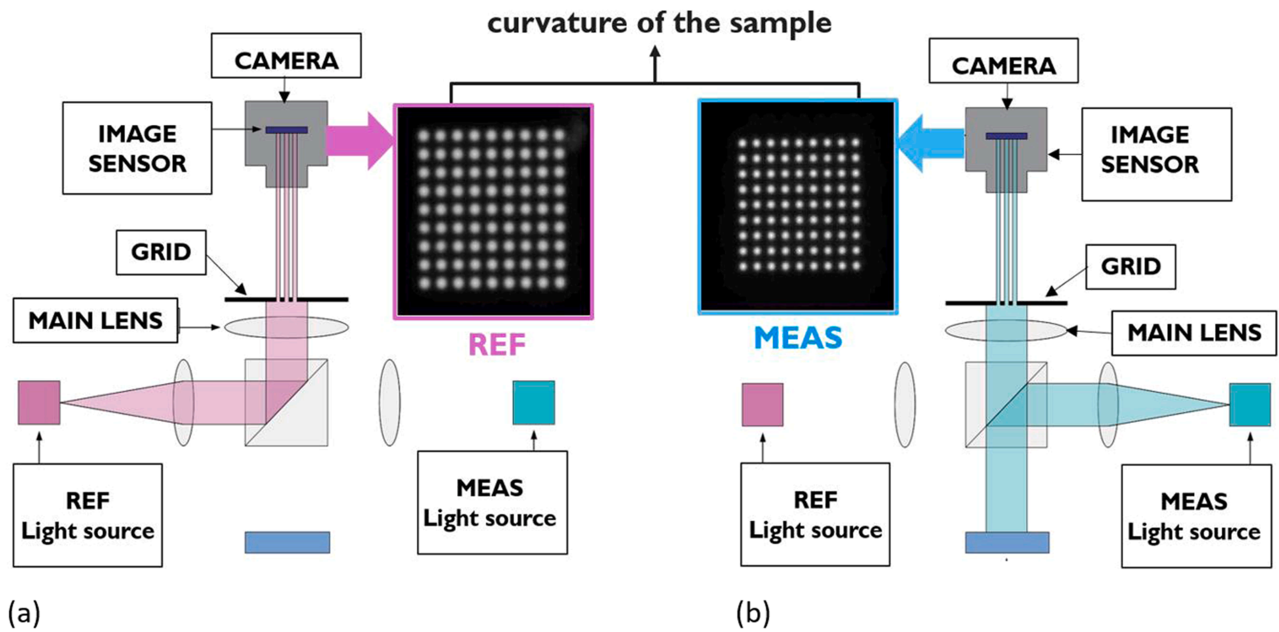

Fig. 1. experimental setup of the curvature measurements; (a) The reference (REF) light is used to reduce the impact of the imperfections or changes of the GRID; (b) The measurement (MEAS) light is projected and reflected from the sample and it is influenced by the curvature of the sample.

projected on the sample, reflected, patterned by the GRID and captured by the camera to obtain the size of the image. Further comparison of the two images (REF and MEAS) allows to determine the curvature of the sample. To reduce the sensitivity to the external light, an image of the background is captured with both light sources switched off. The background image is then subtracted from the REF and MEAS images and the resulting images are used for the determination of the spots' positions. The REF image is taken to find the actual positions of the spots at the time of the curvature measurement, to avoid errors caused by the thermal expansion of the GRID. The actual distance between holes in the GRID (metal mesh) can slightly vary. A use of the REF image allows to minimize the impact of the GRID manufacturing imperfections.

Results and discussion

Fig. 2 illustrates the measured elastic modulus by nanoindentation and the corresponding thermal film stress change for a temperature range between 25 °C and 200 °C. The stress of thin films on a substrate is determined by curvature measurements and the Stoney's equation [18]

$$\sigma = \left(Es\, t_s^2\right)\circ\left(\frac{1}{R}-\frac{1}{R_0}\right) \quad (4)$$

where R_0 is the radius of curvature of the bare substrate and R is the radius of curvature with the film on the substrate. E_s and ν_s are respectively the elastic modulus and Poisson ratio of the substrate and t_s and t_f are the thicknesses of the substrate and the film, respectively.

The thermal film stress is mainly generated by the difference in the CTE between the film and the substrate and by the elastic modulus of the film. From the nanoindentation measurements, it is found that the elastic modulus is relatively constant in case of OSG 3.0 and OSG 3.2 low-k materials within the temperature range between 25 °C and 150 °C. At temperatures above 150 °C, a significant 10% of increase in elastic modulus was observed. This means that either the elastic modulus of the film changes at temperatures above 150 °C or the measured value by nanoindentation is affected by changes in the residual film stress (Fig. 2b). It is important to mention that the CTE can only be extracted when the elastic modulus in a certain temperature range remains constant and the stress changes linearly with temperature. Therefore, for temperatures above 150 °C, no CTE extraction was possible. This emphasizes the importance of measuring the elastic modulus in the desired temperature range and by doing so selecting the correct temperature range for CTE extraction.

As shown on Fig. 2b, a bi-linear behavior of the film stress with temperature was found, with a transition around 100 °C. Since the elastic modulus is found not to significantly change within the temperature range of 25 °C and 150 °C (Fig. 2a), this suggests that this bi-linear behavior may be caused by a change in the difference between the CTE of the film and the substrate. Although the thermal expansion coefficients of solids usually show little dependence on temperature (except at very low temperatures), it is known that the CTE of silicon for instance changes from 2.6 ppm/ °C at room temperature to respectively 3.1 ppm/ °C at 100 °C and 3.3 ppm/ °C at 150 °C [19]. This may complicate the calculation of the CTE of the OSG materials. For simplicity, the CTE of the OSG films was therefore calculated in a temperature range between 25 °C and 100 °C and by assuming a constant value of 2.6 ppm/ °C for silicon. Another potential reason for a bi-linear behavior of the film stress with temperature could be related to a change in plasticity of the OSG films at elevated temperatures.

Fig. 3 shows the experimentally obtained curvature and FEM result in case of a 300 nm SiO_2 film and OSG 3.2 low-k film on top of a thinned Si substrate for the temperature range between 25 °C and 100 °C. Measuring the curvature as a function of temperature allows the calculation of the film's CTE directly. The CTE at a specific temperature is determined using Hooke's law (σ= εE, where ε is calculated as $\varepsilon_{th}=\alpha\Delta T$) and by observing the curvature variation over some change in temperature using the Stoney equation. Note that the elastic modulus value is required as input, which was measured by nanoindentation (Fig. 2a). Moreover, because the substrates of the samples were thinned to about 100 μm, any small variation in substrate thickness may impact the accuracy of the film stress calculated using the Stoney equation. Therefore, the substrate thickness was accurately measured for each sample using a digital micrometer system Digimicro ME-50H. Moreover, by thinning down the substrate, the film to substrate ratio is increased to about 0.3%, which may question the use of the Stoney equation. Finite element simulations were therefore performed to study the validity of the Stoney equation using a thinned substrate and in order to fully account for the rectangular geometry of the sample, instead of the uniform curvature that is assumed by the Stoney equation. For each

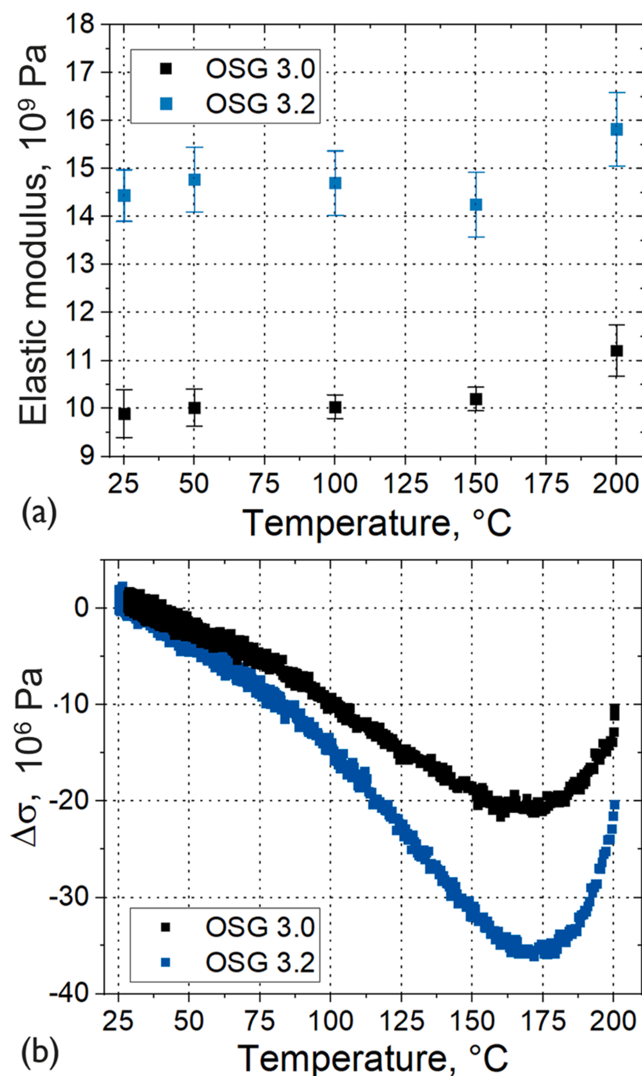

Fig. 2. (a) measured elastic modulus of 300 nm thickn OSG 3.0 and OSG 3.2 low-k films as a fuction of temperature, assuming a Poisson's ratio of 0.3 for each temperature ranging from 25 °C to 200 °C and (b) the calculated stress change based on the Stoney equation in a temperature range from 25 °C to 200 °C.

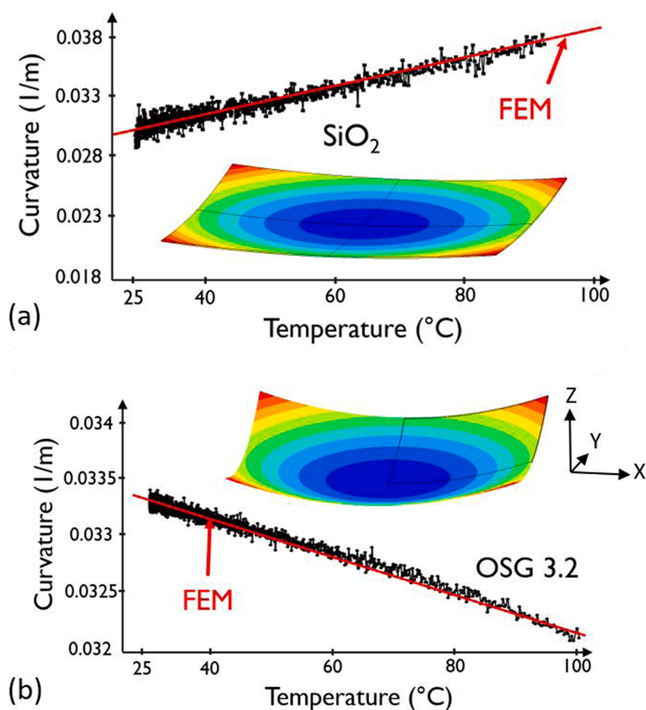

Fig. 3. Experimental and FEM fit of the curvature in case of a 300 nm SiO2 film and an OSG 3.2 low-k film on top of a thinned Si substrate.

experimentally obtained curvature versus temperature data set, several FEM computations were performed using different values of the CTE, until the best fit of the experimental values of curvature was found. Table 1 summarizes the extracted CTE values obtained using FEM and Hooke's law (σ= εE, where ε is calculated as $\varepsilon_{th}=\alpha\Delta T$). As shown, good agreement was found between Hooke's law and FEM

From the obtained CTE values by measuring the curvature as a function of temperature, the change in critical crack initiation force with the change in film stress (parameter A_1 in Eq. (3)), for two different indenter probe geometries could be obtained (Table 2). This was done by comparing the measured change in F_{crit} with temperature using nano-indentation with the film stress change with temperature using curvature measurements as shown on Fig. 4. For SiO_2 films, only the force-displacement curves retrieved using a 60° pyramidal probe showed a critical crack initiation force. This is because for the 90° pyramidal probe geometry, the stresses upon indentation are not sufficient to initiate cracks, while for the 60° pyramidal probe, the indentation stress is much larger.

To further elaborate the relationship between the elastic modulus and A_1, three OSG films with different levels of porosity and elastic modulus were fabricated using the alternative manufacturing sequence, as proposed by Urbanowicz et al. [20]. Fig. 5 shows the measured elastic modulus and matrix density as a function of film porosity for respectively OSG 2.1, OSG 2.3 and OSG 2.5 films.

The matrix density of the low-k films was calculated based on the mass, thickness and open porosity measurements. The mass was measured with a high resolution, in-line mass measurement system with an accuracy better than 0.1 mg, while the thickness and open porosity of the films were measured by ellipsometric porosimetry. As shown on Fig. 5, films with different elastic modulus and porosity, but similar matrix density were obtained. It was demonstrated by Vanstreels and co-authors that a similar matrix density for different levels of porosity suggests that the stiffness of the organosilicate matrix does not vary with porosity and that no significant differences in cross-linkage are expected for films with for different levels of porosity [9]. Theoretically, different levels of porosity should not affect the CTE of the material if the matrix material is the same. Therefore, by taking the measured values for A_0 for respectively OSG 2.1, OSG 2.3 and OSG 2.5 and assuming the same CTE value for the 3 films, the corresponding A_1 factor could be estimated. As shown on Fig. 6, the calculated values for A_1 and the corresponding elastic modulus values follow the same relationship as for the values reported in Table 2. Fig. 7 shows the impact of the probe geometry on the relationship between A_1 and the elastic modulus in case of a 60° and 90° pyramidal probe. In both cases, A_1 scales linearly with elastic modulus. At first sight, one could argue that this dependency puts stringent demands on the extraction of the CTE because even two indenter probes with similar probe geometry are never identically fabricated. Moreover, the probe geometry may also be altered due to extensive use of it at elevated temperatures. However, by re-measuring how F_{crit} of OSG 3.0, OSG 3.2 and SiO_2 changes with temperature (A_0) for a specific probe geometry that is used, and by using the measured values of Δσ/ΔT for those corresponding films, one could recalibrate the A_1 versus elastic modulus relationship each time a new indenter probe is installed. Moreover, this calibration methodology is not limited to low-k dielectrics but can also be expanded to a wider range of dedicated materials.

Table 1
comparison between the CTE values obtained with FEM and Hooke's law. The indicated error values are the standard deviations. These values were determined from 10 measurements.

Material	Substratethickness,µm	Filmthickness,nm	Filmstress,MPa	Elasticmodulus, 10^9 Pa	Poisson'sratio	CTE, ppm/ °C(FEM)	CTE, ppm/ °C(Hooke's law)
SiO_2	103 ± 2	300 ± 5	−143 ± 6	70 ± 2	0.17	0.92 ± 0.15	0.89 ± 0.16
OSG 3.0	102 ± 2	300 ± 5	47 ± 2	10.2 ± 0.5	0.3	10.95 ± 0.45	10.51 ± 0.54
OSG 3.2	101 ± 2	300 ± 5	35 ± 2	15.1 ± 0.8	0.3	11.72 ± 0.66	11.70 ± 0.42

Table 2
calculated change in critical crack initiation force, F_{crit}, with the change in film stress for two different indenter probe geometries. The calculations are based on the experimentally measured change in F_{crit} with temperature by nano-indentation and the measured film stress change with temperature using curvature tests.

Material	Elasticmodulus,10^9 Pa	$\Delta F_{crit}/\Delta\sigma$,$10^{-12}$ N/Pa	Indenter probegeometry
SiO_2	70 ± 2	−31.042	60° Pyramid
		n.a.	90° Pyramid
OSG 3.0	10.2 ± 0.5	−2.184	60° Pyramid
OSG 3.0		−13.598	90° Pyramid
OSG 3.2	15.1 ± 0.8	−4.719	60° Pyramid
OSG 3.2		−19.426	90° Pyramid

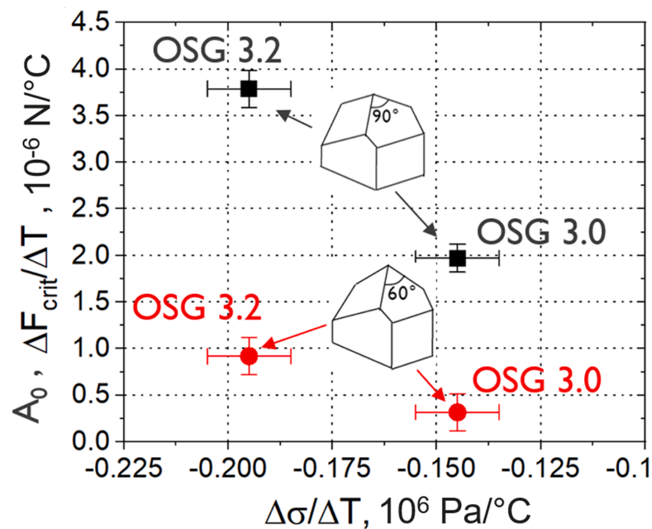

Fig. 4. Experimentally obtained change in critical crack initiation force with the change in film stress (A_0) versus the for two different indenter probe geometries.

Conclusions

To summarize, a nanoindentation based method was demonstrated to determine the thermal expansion coefficients of low-k dielectrics. This methodology was calibrated using curvature measurements to elucidate the impact of tip geometry and elastic modulus on the theoretical model to calculate the CTE. By using the measured Δσ/ΔT values for a set of calibration samples, the relationship between A_1 and the elastic modulus can be calibrated each time a new indenter probe geometry is used or the probe geometry is altered by intensive use. The advantage of this methodology over other techniques is the capability to simultaneously measure the elastic modulus, the easy sample preparation, short measurement time and easy analysis. Using this approach, the CTE of a wide range of materials could be estimated.

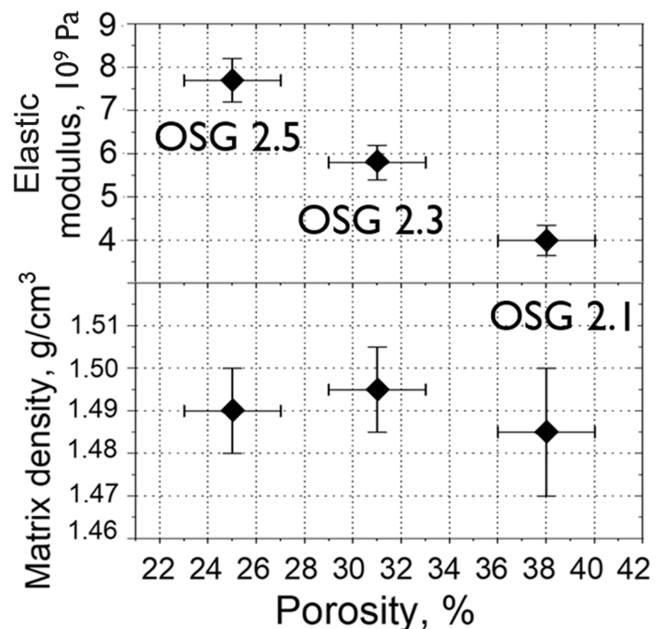

Fig. 5. Elastic modulus and matrix density as a function of the film's porosity in case of OSG 2.1, OSG 2.3 and OSG 2.5 low-k films.

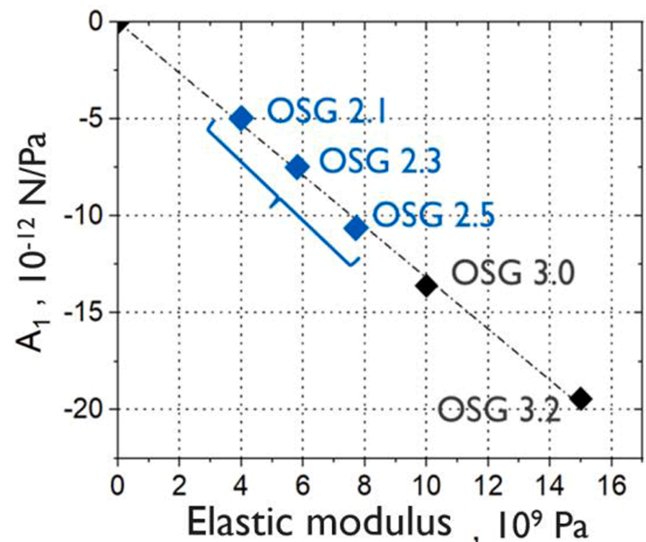

Fig. 6. Experimentally obtained A_1 as a function of the film's elastic modulus.

Conflict of interest statement

On behalf of all authors, the corresponding author states that there is no conflict of interest.

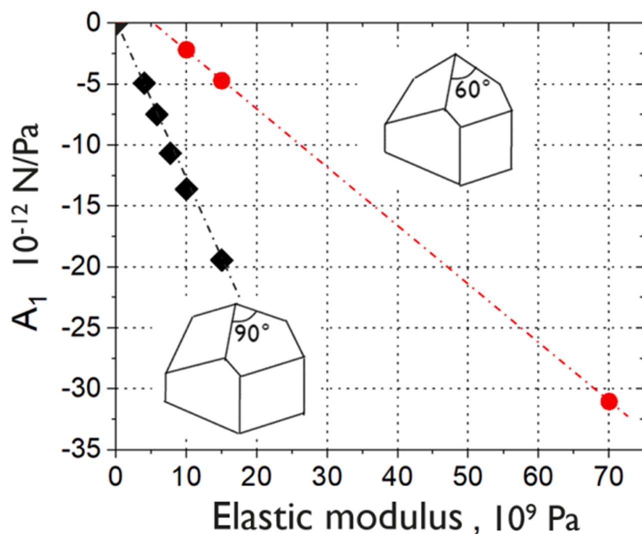

Fig. 7. impact of probe geometry on the dependency of A_1 on the film's elastic modulus.

Data availability statement

All data generated or analysed during this study are included in this published article.

CRediT authorship contribution statement

Kris Vanstreels: Conceptualization, Methodology, Investigation, Validation, Writing – original draft, Writing – review & editing. **Abdellah Salahouelhadj:** Software, Validation, Investigation. **Mario Gonzalez:** Supervision.

Declaration of Competing Interest

The authors declare that they have no known competing financial interests or personal relationships that could have appeared to influence the work reported in this paper.

Data Availability

No data was used for the research described in the article.

References

[1] J.D. Meindl, Beyond Moore's Law: the interconnect era, Comput. Sci. Eng. 5 (2003) 20–24. https://ieeexplore.ieee.org/document/1166548.

[2] J.S. Clarke, C. George, C. Jezewski, A. Maestre Caro, D. Michalak, J. Torres, Process technology scaling in an increasingly interconnect dominated world, IEEE Sympos. VLSI Technol.-Tech. Digest 1 (2014) 1–2. https://ieeexplore.ieee.org/document/6894407.

[3] M.R. Baklanov, C. Adelmann, L. Zhao, S. de Gendt, Advanced interconnects: materials, processing, and reliability, ECS J. Solid State Sci. Technol. 4 (2015) Y1–Y4. https://iopscience.iop.org/article/10.1149/2.0271501jss.

[4] C.S. Pai, P.W. Diodato, R. Liu, A case study of RC effects to circuit performance, in: Proceedings of the IEEE 1998 International Interconnect Technology Conference, 1998, 6134961. https://ieeexplore.ieee.org/document/704911.

[5] K. Maex, M.R. Baklanov, D. Shamiryan, F. Iacopi, S.H. Brongersma, Z. S. Yanovitskaya, Low dielectric constant materials for microelectronics, J. Appl. Phys. 93 (2003) 8793, https://doi.org/10.1063/1.1567460.

[6] V.Mc Gahay, Porous dielectrics in microelectronic wiring applications, Materials (Basel) 3 (2010) 536–562, https://doi.org/10.3390/ma3010536.

[7] K. Vanstreels, C. Wu, M. Baklanov, Mechanical stability of porous low-k dielectrics, ECS J. Solid State Sci. Technol. 4 (2015) N3058–N3064, https://doi.org/10.1149/2.0071501jss.

[8] K. Vanstreels, C. Wu, M. Gonzalez, D. Schneider, D. Gidley, P. Verdonck, M. R. Baklanov, Effect of pore structure of nanometer scale porous films on the measured elastic modulus, Langmuir 29 (2013) 12025, https://doi.org/10.1021/la402383g.

[9] K. Vanstreels, C. Wu, P. Verdonck, M.R. Baklanov, Intrinsic effect of porosity on mechanical and fracture properties of nanoporous ultralow-k dielectrics, Appl. Phys. Lett. 101 (2012), 123109, https://doi.org/10.1063/1.4753972.

[10] F. Iacopi, S.H. Brongersma, B. Vandevelde, M. O'Toole, D. Degryse, Y. Travaly, K. Maex, Challenges for structural stability of ultra-low-k-based interconnects, Microelectron. Eng. 75 (2004) 54–62, https://doi.org/10.1016/j.mee.2003.09.011.

[11] K. Vanstreels, I. De Wolf, H. Zahedmanesh, H. Bender, M. Gonzalez, J. Lefebvre, S. Bhowmick, In-situ scanning electron microscopy study of fracture events during back-end-of-line microbeam bending tests, Appl. Phys. Lett. 105 (2014) 1–4, https://doi.org/10.1063/1.4902516.

[12] H. Zahedmanesh, M. Gonzalez, K. Vanstreels, A numerical study on nano-indentation induced fracture of low dielectric constant brittle thin films using cube corner probes, Microelectron. Eng. 156 (2016) 108–115, https://doi.org/10.1016/j.mee.2016.01.006.

[13] M. Gonzalez, K. Vanstreels, V. Cherman, K. Croes, L. Kljucar, I. De Wolf, Zsolt Tőkei, Mechanical stability of Cu/low-k BEOL interconnects, IEEE Int. Reliab. Phys. Sympos. IRPS (2014), 14468596. Waikoloa, HI, USA, https://ieeexplore.ieee.org/document/6860606.

[14] H. Zahedmanesh, P. Verdonck, M. Gonzalez, K. Vanstreels, Q.T. Le, Mechanical integrity of nano-interconnects as brittle-matrix nano-composites, Theor. Appl. Fract. Mech. 95 (2018) 194–207, https://doi.org/10.1016/j.tafmec.2018.03.003.

[15] D. James, J.A. Spittle, S.G.R. Brown, R.W. Evans, A review of measurement techniques for the thermal expansion coefficient of metals and alloys at elevated temperatures, Meas. Sci. Technol. 12 (2001) R1–R15, https://doi.org/10.1088/0957-0233/12/3/201.

[16] E.G. Wolff, Thermal Expansion of Thin Films: a review, in: Thermal conductivity 24/Thermal Expansion 12, P. S. Gaal and D. A. Apostoloescu, Eds, International Thermal Conductivity Conference 1997, Pittsburg, PA, U.S.A., CRC Press, 1999.

[17] K. Vanstreels, H. Zahedmanesh, U. Hangen, Thermal expansion coefficients of ultralow-k dielectric films by cube corner indentation test at elevated temperatures, Appl. Phys. Lett. 107 (2015), 233101, https://doi.org/10.1063/1.4936996.

[18] G.G. Stoney, The tension of metallic films deposited by electrolysis, Proc. R. Soc., London, Ser. A82 (1909) 172–175, https://doi.org/10.1098/rspa.1909.0021.

[19] H. Watanabe, N. Ymada, M. Okaji, Linear thermal expansion coefficient of silicon from 293 to 1000K, Int. J. Thermophys. 25 (1) (2004) 221–236, https://doi.org/10.1023/B:IJOT.0000022336.83719.43.

[20] A.M. Urbanowicz, K. Vanstreels, P. Verdonck, D. Shamiryan, S. De Gendt, M. R. Baklanov, Improving the robustness of ultralow-k SiOCH plasma enhanced chemical vapor deposition glasses by controlled porogen decomposition prior to UV-hardening, J. Appl. Phys. 107 (2010), 104122, https://doi.org/10.1063/1.3428958.